APPENDIX

The parameters appearing in (5) are

$$\begin{aligned}
\overline{\tilde{\alpha}} &= \begin{bmatrix} \overline{\tilde{\alpha}}_1 \\ \overline{\tilde{\alpha}}_2 \end{bmatrix} \\
\overline{\tilde{\beta}} &= \begin{bmatrix} \overline{\tilde{\beta}}_1 \\ \overline{\tilde{\beta}}_2 \end{bmatrix} \\
\overline{\overline{K}}_M &= \begin{bmatrix} \overline{\overline{K}}_{M,1} & 0 \\ 0 & \overline{\overline{K}}_{M,2} \end{bmatrix} \\
\overline{\overline{P}}_{M-1} &= [\overline{\overline{P}}_{(M-1),1} \quad \overline{\overline{P}}_{(M-1),2}] \\
\overline{\overline{Q}}_{M-1} &= \begin{bmatrix} \overline{\overline{Q}}_{(M-1),1} \\ \overline{\overline{Q}}_{(M-1),2} \end{bmatrix}.
\end{aligned} \tag{6}$$

The (m,n)th element of $\overline{\overline{P}}_{(M-1)\lambda}$ $(P_{(M-1)\lambda,mn})$, the (m,n)th element of $\overline{\overline{Q}}_{(M-1)\lambda}$ $(Q_{(M-1)\lambda,mn})$, and the mth element of $\overline{V}_{M-1}$ $(V_{M-1,m})$ are defined as

$$\begin{aligned}
P_{(M-1)\lambda,mn} &= \frac{2}{b_{M-1}} \int_{c_\lambda}^{c_\lambda+W_\lambda} dx \cdot \sin[\gamma_{(M-1)m}(x+a_{M-1})] \\
&\quad \cdot \sin[\tau_{\lambda n}(x-c_\lambda)] \\
Q_{(M-1)\lambda,mn} &= \frac{2\epsilon_{M-1}\gamma_{(M-1)n}}{W_\lambda \epsilon_M \tau_{\lambda m}} \int_{c_\lambda}^{c_\lambda+W_\lambda} dx \cdot \sin[\tau_{\lambda m}(x-c_\lambda)] \\
&\quad \cdot \sin[\gamma_{(M-1)n}(x+a_{M-1})] \\
V_{M-1,m} &= V_o \frac{2}{b_{M-1}} \int_{c_1+W_1}^{c_2} dx \cdot \sin[\gamma_{(M-1)m}(x+a_{M-1})].
\end{aligned} \tag{7}$$

The $\overline{\overline{P}}_{(M+1)\lambda}$, $\overline{\overline{Q}}_{(M+1)\lambda}$, and $\overline{V}_{M+1}$ are defined in a similar way. $\overline{\tilde{\alpha}}_\lambda$ $(\overline{\tilde{\beta}}_\lambda)$ is the vector consists of $[\tilde{\alpha}_{\lambda 1}, \tilde{\alpha}_{\lambda 2}, \cdots]$ $([\tilde{\beta}_{\lambda 1}, \tilde{\beta}_{\lambda 2}, \cdots])$.

ACKNOWLEDGMENT

The author would like to thank the reviewers for their useful comments.

REFERENCES

[1] T. M. Weller, L. P. B. Katehi, and G. M. Rebeiz, "High performance microshield line components," *IEEE Trans. Microwave Theory Tech.*, vol. 43, pp. 534–543, Mar. 1995.

[2] K. Wu and R. Vahldieck, "The method of lines applied to planar transmission lines in circular and elliptical waveguides," *IEEE Trans. Microwave Theory Tech.*, vol. 37, pp. 1958–1963, Dec. 1989.

[3] F. Medina and M. Horno, "Capacitance and inductance matrices for multistrip structures in multilayered anisotropic dielectrics," *IEEE Trans. Microwave Theory Tech.*, vol. MTT-35, pp. 1002–1008, Nov. 1987.

[4] K.-K. M. Cheng and I. D. Robertson, "Simple and explicit formulas for the design and analysis of asymmetrical V-shaped microshield line," *IEEE Trans. Microwave Theory Tech.*, vol. 43, pp. 2501–2504, Oct. 1995.

[5] ——, "Quasi-TEM study of microshield lines with practical cavity sidewall profiles," *IEEE Trans. Microwave Theory Tech.*, vol. 43, pp. 2689–2694, Dec. 1995.

[6] N. Yuan, C. Ruan, and W. Lin, "Analytical analyses of V, elliptic, and circular-shaped microshield transmission lines," *IEEE Trans. Microwave Theory Tech.*, vol. 42, pp. 855–859, May 1994.

[7] F. Medina and M. Horno, "Spectral and variational analysis of generalized cylindrical and elliptical strip and microstrip lines," *IEEE Trans. Microwave Theory Tech.*, vol. 38, pp. 1287–1293, Sept. 1990.

[8] J. E. Schutt-Aine, "Static analysis of V transmission lines," *IEEE Trans. Microwave Theory Tech.*, vol. 40, pp. 659–664, Apr. 1992.

[9] C. Wei, R. F. Harrington, J. R. Mautz, and T. K. Sarkar, "Multiconductor transmission lines in multilayered dielectric media," *IEEE Trans. Microwave Theory Tech.*, vol. MTT-32, pp. 439–450, Apr. 1984.

[10] T. Itoh, ed., "*Numerical Techniques for Microwave and Millimeter-Wave Passive Structures*." New York: Wiley, 1989.

[11] J. Bornemann, "Scattering-type transverse resonance technique for the calculation of (M)MIC transmission line characteristics," *IEEE Trans. Microwave Theory Tech.*, vol. 39, pp. 2083–2088, Dec. 1991.

[12] J.-F. Kiang, "Capacitance of microstrip lines with inhomogeneous substrate," *IEEE Trans. Microwave Theory Tech.*, vol. 44, pp. 1703–1709, Oct. 1996.

[13] ——, "Quasi-TEM analysis of coplanar waveguides with an inhomogeneous semiconductor substrate," *IEEE Trans. Microwave Theory Tech.*, vol. 44, pp. 1586–1589, Sept. 1996.

Cutoff Frequencies of an Asymmetrically Loaded Cylindrical Waveguide

Tat Soon Yeo

***Abstract*—The cutoff characteristics of an asymmetrically loaded cylindrical waveguide are analyzed using the null-field method. The fields in the metallic waveguide and dielectric loading are expressed in their corresponding guided-wave modes. The addition theorem of the Bessel function is used to relate the fields across the air–dielectric boundary.**

***Index Terms*—Asymmetric loading, cylindrical waveguide.**

I. INTRODUCTION

The computation of the cutoff frequencies and propagation constants of a cylindrical waveguide asymmetrically loaded with a dielectric cylinder has been the subject of much investigations [1], [2]. These research efforts have previously been pioneered by antenna designers interested in synthesizing specific aperture field across a cylindrical radiator; hence, leading to a specific radiation pattern. Lately, the hybrid microwave-integrated-circuit designers interested in accurately modeling the dielectric resonator enclosed within a metallic box are also seriously looking into this problem.

The reported work are often based on the concept of field matching across the air–dielectric boundary. Rothwell *et al.* [1] have used the simple point-matching method, while Yeo [2] has used the method of the least-squares boundary residual. While the legitimacy of the former method has often been called into question [3], the latter is a minimization procedure that has not been shown to be able to lead to a guaranteed global minimum.

On the other hand, the convergence and uniqueness of the null-field method [4] have been well proven [5]–[8]. In 1982, Martin [8] stated categorically that, "we prove that the infinite system of null-field equations always has precisely one solution." In this paper, the null-field method is used to compute the cutoff frequencies of the asymmetrically loaded cylindrical waveguide for both the transverse-electric and transverse-magnetic modes.

As correctly pointed out by Kuttler [9], the cross-sectional geometry of a asymmetrically loaded cylindrical waveguide is not easily

Manuscript received October 21, 1996; revised March 9, 1998.

The author is with the Department of Electrical Engineering, National University of Singapore, Singapore 119260.

Publisher Item Identifier S 0018-9480(98)06154-7.

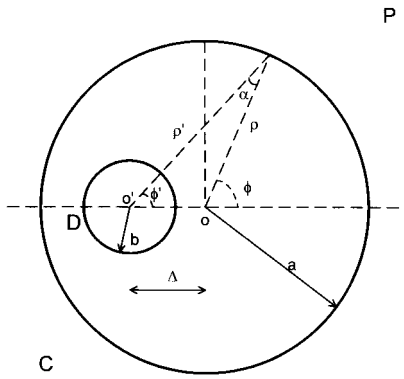

Fig. 1. Geometry of the asymmetrically load cylindrical waveguide. The boundary of the metallic waveguide is C, while the boundary of the dielectric rod is D.

analyzed since it does not readily lend itself to the separation-of-variables scheme of solution. Thus, previous researchers have always resorted to circumvent this difficulty by FORCING the fields to match across the air–dielectric boundary. In this paper the author made use of the well-known addition theorem of the Bessel function [10] to facilitate a rigorous field matching using the orthogonality property of the Bessel functions.

II. Theory

Referring to Fig. 1, the electric field at a point P outside the cylindrical waveguide generated by the equivalent sources on the surface of the dielectric rod and the metallic cylinder must be zero. Therefore, from the null-field method, we have

$$\oint_D [\Psi_D(Q_D)\nabla g(P, Q_D) - g(P, Q_D)\nabla\Psi_D(Q_D)]\underline{n}_D \bullet dC(Q_D) + \oint_C [\Psi_C(Q_C)\nabla g(P, Q_C) - g(P, Q_C)\nabla\Psi_C(Q_C)]\underline{n}_C \bullet dC(Q_C) = 0 \quad (1)$$

where Ψ_D and Ψ_C are the E_z field for the TM mode at cutoff or H_z field for the TE mode at cutoff within the dielectric rod of radius b and the metallic guide of radius a, respectively. ∇ is the gradient operator, g is the two-dimensional free-space Green's function, Q_D and Q_C are points on, and $\underline{n}_D$ and $\underline{n}_C$ are units normal to, the surface of the dielectric rod (D) and metallic guide (C), respectively.

The fields Ψ_D and Ψ_C at cutoff can be expressed in terms of their guided-wave modes as follows:

$$\Psi_D = \sum_n a_n J_n(\nu k_c \rho') F_n(\phi') \exp j(\omega t) \quad (2)$$

$$\Psi_C = \sum_n [b_n J_n(k_c\rho) + c_n Y_n(k_c\rho)] F_n(\phi) \exp j(\omega t) \quad (3)$$

where $\nu = \sqrt{\varepsilon_r}$, (ρ, ϕ, z) are the cylindrical coordinates with respect to the center of the cylindrical waveguide O, (ρ', ϕ', z') are the cylindrical coordinates with respect to the center of the dielectric rod O', a_n, b_n, and c_n are expansion coefficients, and J_n and Y_n are Bessel functions of the first and second kind, respectively,

$$F_n(\phi) = \begin{cases} \cos(n\phi), & \text{even modes} \\ \sin(n\phi), & \text{odd modes} \end{cases}$$

$$c_n = \begin{cases} 0, & \text{if } \Delta > b \\ C_n, & \text{otherwise.} \end{cases}$$

The addition theorem of the Bessel functions is then used to relate the dielectric waveguide fields and metallic waveguide fields as follows:

$$\Phi_n(k_c\rho)F_n(n\phi) = \sum_{m=-\infty}^{\infty} \Phi_{n+m}(k_c\rho')J_m(k_c\Delta)F_{n+m}(\phi'), \quad \text{for } \Delta > \rho' \quad (4)$$

$$\Phi_n(k_c\rho)F_n(n\phi) = \sum_{m=-\infty}^{\infty} \Phi_{n+m}(k_c\Delta)J_m(k_c\rho')F_{n+m}(\phi'), \quad \text{for } \Delta < \rho' \quad (5)$$

for $n = 0, 1, 2, \cdots$, where Δ is the displacement between O and O', and Φ_n could either be the Bessel function of the first or second kind.

By matching the fields and their normal derivatives at $\rho' = b$, and applying the orthogonality property of the Bessel functions, we obtain the following set of equations:

$$a_p J_p(\nu k_c b) = J_p(k_c b)\Sigma b_n J_{p-n}(k_c\Delta) + \delta Y_p(k_c b)\Sigma c_n J_{p-n}(k_c\Delta) \quad (6)$$

and

$$\mu a_p J_p'(\nu k_c b) = J_p'(k_c b)\Sigma b_n J_{p-n}(k_c\Delta) + \delta Y_p'(k_c b)\Sigma c_n J_{p-n}(k_c\Delta) \quad (7)$$

for $p = 0, 1, 2, \cdots$, where

$$\delta = \begin{cases} 0, & \text{if } \Delta > b \\ 1, & \text{otherwise} \end{cases}$$

$$\mu = \begin{cases} \nu, & \text{TM modes} \\ 1/\nu, & \text{TE modes.} \end{cases}$$

Equations (6) and (7) form a set of homogeneous simultaneous equations. The solution to this set of equations is nonzero if and only if the determinant of the coefficient matrix is equal to zero. Therefore, the cutoff frequency could be determined by simply performing a one-dimensional search with its upper and lower bounds given by the cutoff frequencies of an empty and a fully loaded waveguide, respectively. The solution is unique and no other minimization criteria were needed to ensure convergence.

III. Results

The rate of convergence of the solution is extremely fast. Table I shows two examples where the residual error is smaller than 90 parts per million (ppm) (0.009%) for Case I ($b = 4.75$ mm, $\Delta = 3.5$ mm) using only three modes and 67 ppm for Case II ($b = 5.00$ mm, $\Delta = 3.5$ mm) using only four modes, respectively. The diameter of the cylindrical waveguide used is 19 mm and the dielectric constant of the dielectric rod is 2.58.

The cutoff frequencies for the TM_{01}, TM_{11}, TE_{11}, and TE_{21} modes of a concentrically loaded cylindrical waveguide (i.e., for the case $\Delta = 0$) were evaluated using this method for various values of b/a. The results obtained were found to *agree exactly* with the theoretical values obtained using the method of separation of variables.

Figs. 2 and 3 show the variation of the respective TM and TE modes cutoff frequencies versus displacement Δ/a for various sizes of the dielectric rod ranging from 5 to 8 mm radius. The dielectric constant used is 2.58 and the radius of the cylindrical waveguide is 9.5 mm. It is clear from Figs. 2 and 3 that when Δ/a approaches zero, the cutoff frequencies approach the cutoff frequencies of the concentrically loaded waveguide. Again, at $\Delta = 0$, the cutoff frequencies *agree exactly* with those obtained from the method of separation of variables. It is interesting to note that asymmetrical loading has a lesser effect on the cutoff frequencies of the TE modes than that of the TM modes. This could be attributed to the fact that the

TABLE I
CONVERGENCE OF NUMERICAL RESULTS $a = 9.5$ mm, $\varepsilon_r = 2.58$, $\Delta = 3.5$ mm. CASE I: $b = 4.75$ mm, CASE II: $b = 5.00$ mm

# of modes used	Frequency (GHz)
Case I	
1	8.682589118
2	8.768228663
3	8.767415418
4	8.767440216
5	8.767440965
6	8.767440985
7	8.767440983
Case II	
1	8.810694932
2	8.593465517
3	8.668228657
4	8.667644419
5	8.667661952
6	8.667662263
7	8.667662251
8	8.667662249

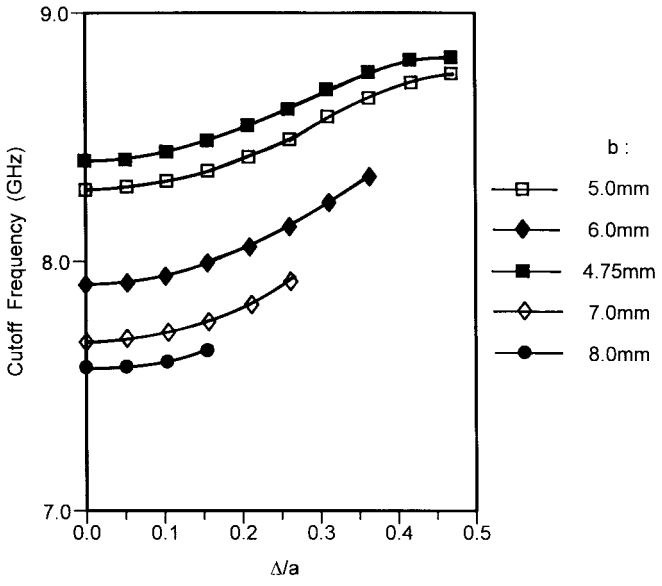

Fig. 2. TM mode cutoff frequencies of an asymmetrically loaded cylindrical waveguide $a = 9.5$ mm and $\varepsilon_r = 2.58$.

boundary conditions for the TM modes require the tangential electric field (E_z) to be zero at $\rho = a$, while the boundary conditions for the TE modes require only $\partial H_z/\partial n = 0$ at $\rho = a$.

A metallic cylindrical cavity of 19-mm diameter and 5-mm height was fabricated. A Teflon rod of 2.006 dielectric constant, 5-mm lengths, and 9.5-mm diameter was also fabricated and inserted into the cylindrical cavity at various displacement positions. The measured resonant frequencies comparing with the computed results are tabulated in Table II. It is observed that the difference is well within 2% and is lowest for the case of symmetrical loading (0.12% error). The measurement error can be attributed to many sources, mainly the loading effect of the coupling holes, error in placing the Teflon rod at the exact positions, and error in measuring the dielectric constant of Teflon. The error is also higher at a smaller value of Δ/a and when Δ/a approaches 0.5 (when the Teflon rod is touching the cavity wall). For the former, the error in positioning the Teflon rod is likely to be the cause. On the other hand, the concentration of the electric field adjacent to the cavity wall (and, hence, coupling holes) is likely to increase the loading effect and, hence, raise the measurement error for the latter.

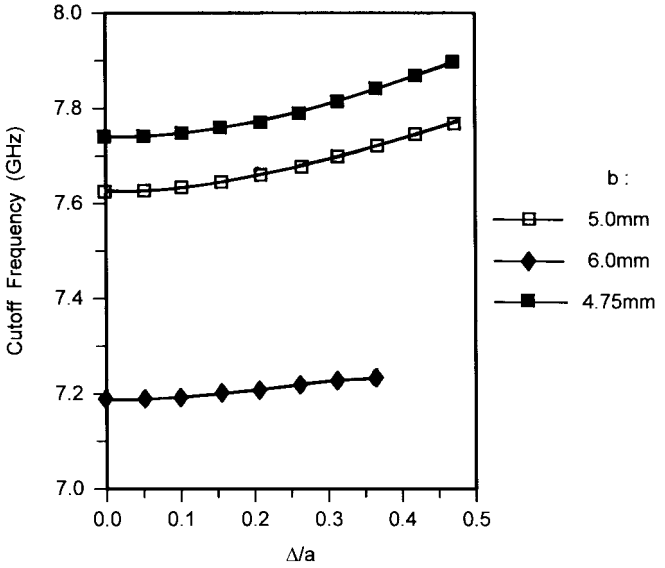

Fig. 3. TE mode cutoff frequencies of an asymmetrically loaded cylindrical waveguide $a = 9.5$ mm and $\varepsilon_r = 2.58$.

TABLE II
COMPARISON BETWEEN MEASURED AND PREDICTED RESONANT FREQUENCIES OF A LOADED CYLINDRICAL CAVITY $a = 9.5$ mm, $b = 4.75$ mm, $\varepsilon_r = 2.006$

Offset from centre Δ/a	Cutoff frequency (measured GHz)	Cutoff frequency (computed GHz)	Error %
0.00	9.187	9.198	0.12
0.10	9.066	9.235	1.83
0.20	9.169	9.330	1.73
0.30	9.417	9.528	1.16
0.40	9.661	9.794	1.36
0.50	9.902	10.072	1.68

IV. CONCLUSION

In this paper, we have introduced an ingenious method of matching the fields across the air–dielectric boundary in an asymmetrically loaded cylindrical waveguide. The use of the addition theorem of the Bessel functions eliminated the needs to force–match the fields either by point-matching or by least square boundary residual (LSBR), thereby improving the overall numerical accuracy and efficiency. It is clear from (6) and (7) that the matching of both the fields and their derivatives also ensure a smoother transition across the air–dielectric

boundary. Examples given in Table I clearly show the efficiency of this method, with the residual error smaller than 100 ppm (0.01%), using only three to four modes in each region of the waveguide.

REFERENCES

[1] E. J. Rothwel and L. L. Frasch, "Propagation characteristics of dielectric-rod-loaded waveguides," *IEEE Trans. Microwave Theory Tech.,* vol. 36, pp. 594–600, Mar. 1988.

[2] S. P. Yeo, "Application of least–squares boundary residual method to the analysis of a circular waveguide loaded with nonconcentric dielectric rod," *IEEE Trans. Microwave Theory Tech.,* vol. 38, pp. 1092–1095, Aug. 1990.

[3] J. B. Davies and P. Nagenthiram, "Irregular fields, nonconvex shapes and the point-matching method for hollow waveguides," *Electron. Lett.,* vol. 7, pp. 401–404, July 1971.

[4] R. H. T. Bates, "General introduction to the extended boundary condition," in *Acoustic, Electromagnetic and Elastic Wave Scattering—Focus on the T-Matrix Approach*, V. K. Varadan and V. V. Varadan, Eds. New York: Pergamon, 1980, pp. 21–31.

[5] A. G. Ramm, "Justification of the T-matrix approach," in *Antennas Propagat. Int. Symp. Dig.,* Albuquerque, NM, 1982, pp. 13–14.

[6] ——, "Convergence of the T-matrix approach to scattering theory," *J. Math. Phys.,* vol. 23, no. 6, pp. 1123–1125, June 1982.

[7] D. Colton and R. Kress, "The unique solvability of the null field equations of acoustics," *Q. J. Mech. Appl. Math.,* vol. 36, pt. 1, pp. 87–95, Jan. 1983.

[8] P. Martin, "Acoustic scattering and radiation problems, and the null-field method," *Wave Motion,* pp. 391–408, Apr. 1982.

[9] J. R. Kuttler, "A new method for calculating TE and TM cutoff frequencies of uniform waveguides with lunar or eccentric annular cross section," *IEEE Trans. Microwave Theory Tech.,* vol. 32, pp. 348–353, Apr. 1984.

[10] M. Abramowitz and I. A. Stegun, *Handbook of Mathematical Functions.* New York: Dover, 1965.

3-D FEM/BEM—Hybrid Modeling of Surface Mounted Devices Within Planar Circuits

T. F. Eibert and V. Hansen

***Abstract*— Three–dimensional (3-D) finite-element (FE) meshes of surface-mounted devices (SMD's) are combined with the surface-current models of planar circuits in multilayered media. This is accomplished on the basis of Huygens' principle via the introduction of equivalent electric and magnetic surface-current densities on a surface enclosing the 3-D parts of the SMD's. The fields in the layered media are described by a surface integral equation based on the dyadic Green's function of the layered media. Special attention is directed to a proper interface of the surface and 3-D parts of the models. Numerical results for a homogeneous and a multilayered capacitor in a microstrip circuit are presented.**

***Index Terms*— Capacitors, finite-element methods, integral equations, nonhomogeneous media.**

Manuscript received October 29, 1997; revised April 3, 1998.

T. F. Eibert is with the Radiation Laboratory, Electrical Engineering and Computer Science Department, University of Michigan, Ann Arbor 48109-2122 USA

V. Hansen is with the Lehrstuhl für Theoretische Elektrotechnik, Bergische Universität/GH Wuppertal, 42119 Wuppertal, Germany.

Publisher Item Identifier S 0018-9480(98)06155-9.

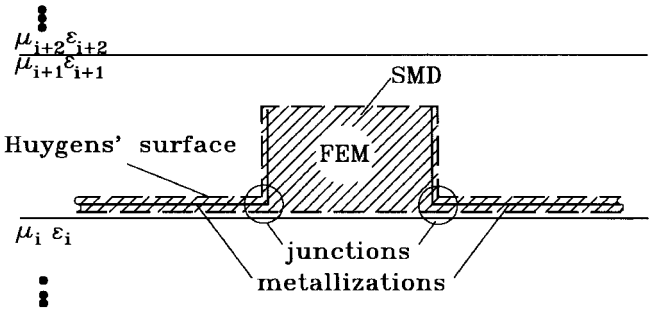

Fig. 1. Model of the field problem.

I. INTRODUCTION

Numerical modeling of circuits within multilayered media based on the analytic Green's-function description of the layered structure is usually restricted to the modeling of planar circuits or so-called two-and-one-half dimensional (2.5-D) circuits [1]. In [2] and [3], a hybrid method was presented, which combines the finite-element method (FEM) for the modeling of three-dimensional (3-D) inhomogeneities with a boundary-element method (BEM) for multilayered media. The investigated field problems where restricted to configurations where the 3-D finite-element (FE) models and surface-current models for metallic structures had no direct connection between each other. In this paper, it is illustrated how this method can be applied to modeling of surface-mounted devices (SMD's) within their planar-circuit environment. For this purpose, a connection between the surface-current models of the metallic parts of the circuits and the 3-D FE models of the SMD's is introduced. Numerical results for a homogeneous SMD capacitor and a multilayered SMD capacitor are shown.

II. FORMULATION

The model of the considered field problem is shown in Fig. 1. All disturbances of the multilayered structure are enclosed by a Huygens' surface. On the Huygens' surface, electric and magnetic surface-current densities are introduced according to

$$\vec{J}_A(\vec{r}) = \vec{n}(\vec{r}) \times \vec{H}(\vec{r}) \quad \vec{M}_A(\vec{r}) = -\vec{n}(\vec{r}) \times \vec{E}(\vec{r}). \tag{1}$$

This means that on metallizations, only electric surface-current densities are present. Further, the electric surface-current densities on the lower and upper parts of the Huygens' surface at the metallizations can be added for metallizations with vanishing thickness and be interpreted as the physical electric surface-current density within the metallization.

The fields of the Huygens' current densities within the multilayered medium are described with a surface integral representation, whereas the fields in the SMD are modeled by the FEM. The connection between the two different field formulations are given by the boundary conditions for the tangential-field components on the Huygens' surface. Further details of the basic formulation of the method can be found in [2] and [3].

For the discretization of the model, care must be taken so that Kirchhoff's current-continuity formula is satisfied at the junctions between the metallizations and SMD. In typical edge-based discretization meshes, this is a problem because only one edge is generated at the junctions where three triangles meet. That is, only one independent current will be present at the junction if one unknown